Packaging and Performance of High Power Semiconductor Lasers of High Heat Flux up to 2000 W/cm^2

Xingsheng Liu, Lawrence C. Hughes, Michael H. Rasmussen, Martin H. Hu, Venkata A Bhagavatula, Ronald W. Davis, Catherine G. Caneau, Rajaram Bhat and Chung-En Zah
Corning Inc.,
Science & Technology Center, SP-PR-02-1, Corning, NY 14831, U.S.A,
Email: liux2@corning.com; Phone: 607-248-1110

Abstract

High power broad area semiconductor lasers have found increasing applications. Compared to low power narrow-stripe semiconductor lasers, packaging including the assembly design, process and thermal management, has much higher impact on the output power and reliability of high power broad area lasers which generate more heat and have high heat flux. In this paper, we will first introduce the package structures and assembling process of high power broad area lasers. We will report two types of high power broad area laser assemblies. One is a microchannel liquid cooled assembly and the other is a conduction cooled CT-mount assembly. The performances including output power, thermal behavior and far fields will be presented. The measurement results showed that excellent thermal management through package structure design as well as quality die attachment is the key in not only improving output power, but also significantly improving beam divergence and far field distribution. The reliability of indium solder bonded and AuSn solder bonded CT mount assemblies were evaluated. The results showed that the die attach solder can significant impact the reliability of high power broad area lasers and that indium solder is not suitable for high power laser applications due to electromigration at high current densities and high temperatures.

Key words: semiconductor laser; broad area laser; heat flux; thermal management; far field; beam divergence; reliability.

Introduction

High power broad area semiconductor lasers have found increasing applications in pumping of solid state laser systems and fiber amplifiers, frequency doubling, medical systems and material processing, such as welding, cutting and surface treatment. The performance and reliability of a semiconductor laser are greatly affected by the package structure and thermal property. A laser's maximum optical power is often limited by either thermal rollover or irreversible catastrophic optical mirror damage (COMD) caused by large localized heating at the facet. The threshold current of a laser increases exponentially with the junction temperature while the slope efficiency decreases exponentially with temperature. It is well known that the reliability of a semiconductor laser is strongly affected by the temperature rise in the active region as the operating lifetime of the device decreases exponentially with temperature. Moreover, thermal stresses caused by the package structure and the packaging process itself should be minimized since excessive thermal stresses can affect laser beam quality and reliability. Compared to low power narrow-stripe semiconductor lasers, packaging including the assembly design, process and thermal management, has much higher impact on the out power and reliability of high power broad area lasers since they generate more heat and have high heat flux, e.g., a 1530nm laser could generate up to 30W heat from a single emitter and have heat flux up to 2000 W/cm^2.

Epi-down bonding of semiconductor lasers can significantly reduce the thermal resistance as the epitaxial layers containing the active region are typically much thinner than the substrate [1-3]. For high power broad area lasers, epi-down bonding is especially important. Figure 1 illustrates the detailed schematic structure of an epi-down bonded laser chip on a mounting substrate (it could be a microchannel liquid cooler or a CT mount). The active region is sandwiched in between the cladding layers. The semiconductor substrate side is the n-side and n-metallization is on top of the semiconductor substrate for ohmic contact and n-side connection. The heat is primarily generated inside the active region of the laser diode. The heat flows through the cladding layer, epi-side metallization and down to the die attach solder layer and mounting substrate. The insulation layer (Si_3N_4 is commonly used) is normally very thin, in the order of low sub-micrometer range. The epi-side metallization, especially the Au layer, could have significant effect on the thermal behavior of the laser diode as the thermal conductivity of Au is fairly high (315 W m^{-1}K^{-1}) and it is very close to the heat source [4]. In semiconductor laser packaging, typically either AuSn or indium solder is used as die attachment material. Materials of high thermal conductivity are selected as the mounting substrate, such as AlN, CuW and Cu.

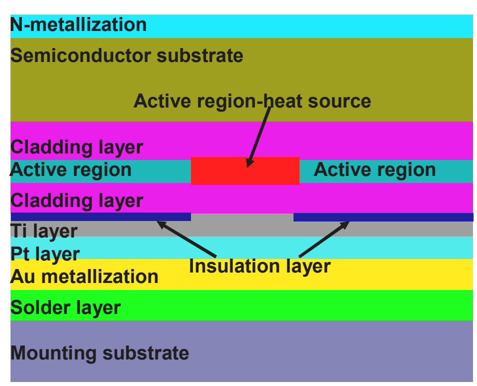

Figure 1. Schematic structure of an epi-down bonded semiconductor laser.

In this paper, we will first introduce the package structures and assembling process of high power broad area lasers. We will report two types of high power broad area laser assemblies. One is a microchannel liquid cooled assembly and the other is a conduction cooled CT-mount assembly. The performances including output power, thermal behavior and far fields will be presented. We will study the influence of package structure on the optical output power, thermal behavior and far fields of high power broad area lasers. The reliability of indium solder bonded and AuSn solder bonded CT mount assemblies were evaluated and the results will be reported.

Package Structure and Process

The CT mount open package is one of the standard broad area laser packages available commercially. Figure 2 shows schematic drawing of a CT mount broad area laser package. The laser chip is epi-down mounted onto a substrate which is the p-side connection. A flylead is attached to the substrate to serve as the n-side connection. Normally the n-side of the chip is wire bonded to the flylead. Figure 3 shows the schematic drawing of a microchannel liquid cooled broad area laser package. The laser chip is mounted onto the microchannel liquid cooler. The n-side connection is made by wire bonding the n-metal of the laser chip to a substrate placed on top of the liquid cooler.

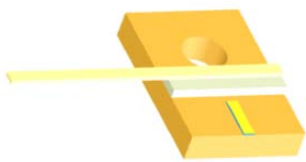

Figure 2. Schematic drawing of a CT mount broad area laser package.

Figure 3. Schematic drawing of a microchannel liquid cooled broad area laser package.

An important element of laser diode packaging is the die bonding of the laser chip to a substrate. The die bonding solder interface and the substrate should offer stable mechanical support, low resistance electrical connection and effective heat sinking to the laser chip. The quality of the die bonding is critical to the operation and reliability of the laser diodes since it can affect the electrical, thermal, and optical properties of the device. The solder material, bonding substrate and the die bonding process are the key factors in achieving quality die bonding with no or few voids, low stress and stable high precision alignment.

Solder and bonding substrate materials have significant impact on laser die bonding quality, performance and stability. To achieve the reliability requirements and reliable laser performances, the bonding stress has to be reduced down to a certain level. Soft solders such as indium solder can relax the stress, have low melting temperature and easy to use. Indium solder has been fairly widely used for broad area laser packaging commercially although there have been some concerns related to migration and whisker formation which could lead to laser degradation or catastrophic failure of the chip [5]. AuSn eutectic solder, which has a melting temperature of 283 °C, is also widely used for laser die attachment. In this paper, both indium and AuSn solders were used. In order to obtain uniform solder interface, reduce solder voids, prevent solder from obscuring the laser facets and make it easier to align the chip to the bonding substrate, deposited AuSn and indium solder films were used instead of solder preforms. The thickness of the AuSn and indium solder films was strictly controlled to be 5 μm. Since the ductility of AuSn solder is very low, a bonding substrate material with CTE matched to that of the laser chip is preferred to reduce the thermally induced bonding stress. Also the bonding substrate should have high thermal conductivity to provide good heat sinking. In our study, the material of CT mount was CuW, which has a thermal conductivity of ~220 W/mK and CTE of $7.5*10^{-6}$/K. The microchannel liquid cooler was made of Cu which has a thermal conductivity of ~390 W/mK but high CTE of $16.5*10^{-6}$/K.

Since the broad area lasers are epi-down mounted, the alignment of the chip to the carrier (either CT mount or microchannel liquid cooler) is more critical. If the laser diode is placed too far back on the carrier, the light beam will be partially blocked and fiber pigtailing will be impossible since the fiber to laser coupling distance is normally only a few micrometers. If it is overhanging, a hot spot will develop which would degrade the laser performance. The alignment tolerance of the chip to carrier is only a few micrometers and therefore high accuracy tooling is required. In the laser die bonding and assembling process, the chip is vacuum picked up and is four-axis aligned to the edge of the carrier with pre-deposited solder and placed on the carrier. The laser chip was designed to have thick Au plateover to protect the active region from over pressure or even crashing during the placement process as well as reduce the thermal stresses in the active region. To prevent flux residues on laser chips, the die bonding is a fluxless process. In the process of solder reflow, slope of the heating ramp, dwell temperature and time, peak temperature and slope of the cooling ramp play significant roles in reducing mechanical and thermal stresses and achieving chip attach integrity [6]. Figure 4 shows a typical cross section of the laser die attachment AuSn solder interface and a typical SEM image of fracture interface after die shearing test. We can see that the die attach solder interface is fairly uniform across the whole chip width, and the bonding between the solder and epi-side metallization is excellent. Study of the die sheared samples revealed that the samples had good die bonding and solder wettability. The fracture interface is inside the chip which means that the die bonding interface has high strength.

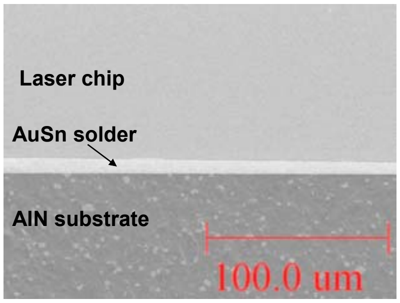

(a)

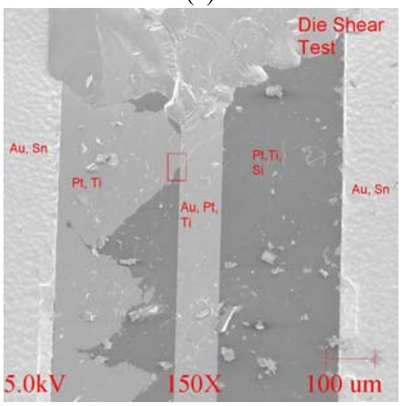

(b)

Figure 4. (a) A typical cross section of the laser chip die attach AuSn solder interface and (b) A typical SEM image of fracture interface after die shearing.

Performances

In this section, the performances such as power-current (LI), wall-plug efficiency, thermal behavior and far fields of 980nm and 1530nm broad area lasers from both microchannel liquid cooled and conduction cooled CT-mount assemblies as well as a fully packaged 980nm laser module will be reported. The study on beam divergence and far field distribution under both CW and pulse operation and the thermal impedances of different packaging configuration will be presented and discussed.

Output Power

Both the 980 nm and 1530nm laser chips are 2mm long and 600 µm wide and have an emitting area width of 120 µm. Figure 5 is the output facet power and wall-plug efficiency of 980nm laser assemblies as a function of CW current measured at room temperature. The high power 980nm broad area laser chips were developed based on the success of single-mode pump lasers [7-8]. A high power of up to 15.3W at 16A was observed from a microchannel liquid cooled package (LC) with the liquid temperature set at 25^{o}C and 9.9W at 12A was obtained from a conduction cooled CT mount package (CT). Under pulsed current condition, over 21W was obtained at 20A. The output power of a microchannel liquid cooled package was limited by COMD and that of the conduction cooled CT mount package was mainly limited by thermal rollover, as can be seen from Figure 5. The maximum wall-plug efficiency is about 66% and 64% at 4A for the microchannel liquid cooled and CT mount packages, respectively. It is obvious that the wall-plug efficiency of the CT mount package drops faster with increasing driving current than that of the microchannel liquid cooled package after reaching peak. Fully packaged fiber pigtailed modules were made using the CT mounts, as shown in Figure 6. The module does not have a TEC (thermoelectric cooler) and the heat removal was achieved by conduction. Figure 7 shows the output power of a pigtailed 980nm laser module with 0.16NA and 100mm core fiber. A high power of 6.5W at 10A was obtained at 25^{o}C. To our knowledge, this is the highest power reported from a 980nm module for a similar chip length and stripe width. Although a 0.16NA fiber was used, high coupling efficiency of >80% below 5A driving current and >75% up to 8A driving current was achieved as a result of a well designed monolithic fiber lens and the small far field angles of the laser chip.

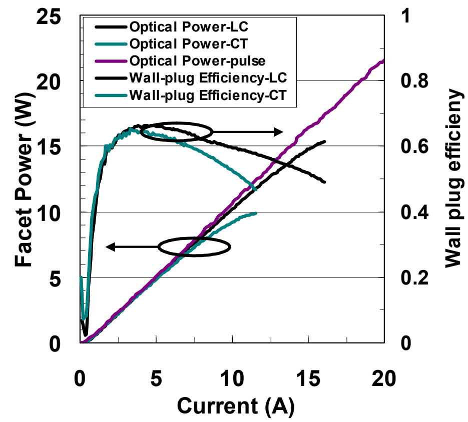

Figure 5. Output facet power and wall-plug efficiency of the 980nm laser assemblies as a function of CW current measured at room temperature.

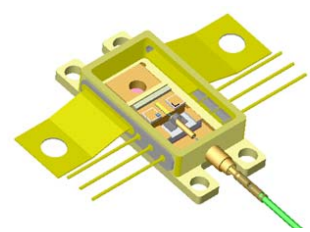

Figure 6. A fully packaged fiber pigtailed 980nm broad area laser module.

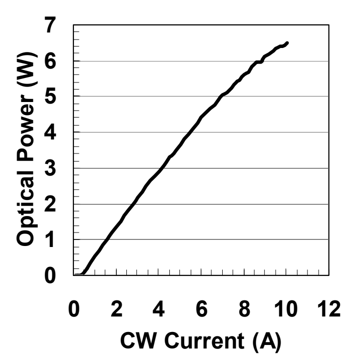

Figure 7. Output power of a fully packaged pigtailed 980nm laser module as a function of CW current measured at 25^{o}C.

For 1530nm lasers, a high power of up to 7.5W at 24A was observed from a microchannel liquid cooled package with the liquid temperature set at 25^{o}C. To our knowledge, this is the highest power reported from a 1530nm laser. 5.1W at 14A was obtained from a conduction cooled CT mount package. Under pulsed current condition, over 15W was obtained at 37A. Figure 8 shows the output facet power and wall-plug efficiency of 1530nm laser assemblies as a function of CW current measured at room temperature. The output power of both assemblies was limited by thermal rollover, as can be seen from Figure 8. COMD is normally not a problem for 1530nm lasers. The maximum wall-plug efficiency of the 1530nm packages is about 36% at 6A which is significantly lower than that of a 980nm laser due to high optical loss and slightly low internal quantum efficiency.

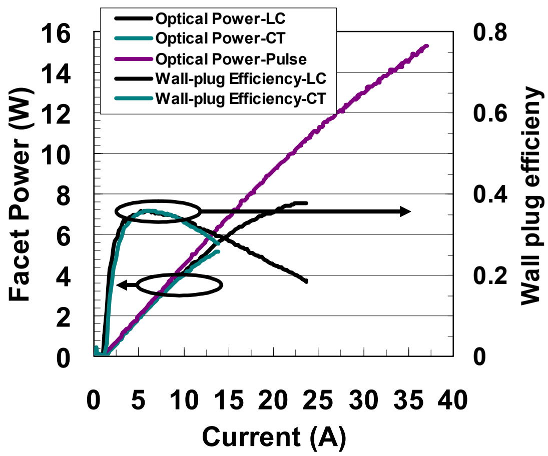

Figure 8. Output facet power and wall-plug efficiency of the 1530nm laser assemblies as a function of CW current measured at room temperature.

Thermal Behavior

The heat generation of the microchannel liquid cooled and conduction cooled CT mount packages of both 980nm and 1530nm lasers can be calculated by Q=IV-L, where Q is the heat generated, I is the driving current and V is the voltage applied on the laser which was measured by four-point method and L is the light output power. Figure 9 is the calculated heat generation of the 980nm laser assemblies as a function of CW current. The microchannel liquid cooled package has about 16W waste heat at the driving current of 16A and the CT mount assembly generates about 11W heat at 12A. The maximum heat flux at the die bonding interface (0.2cm by 0.06 cm) is about 1333 W/cm^2 and 917W/cm^2, respectively, for the microchannel liquid cooled and conduction cooled CT mount packages. From Figure 9 we can see that the heat generation is about the same at currents below 5A and more heat is generated from the CT mount assembly than from microchannel liquid cooled assembly at the same driving current when the current is high. For a 1530nm laser, more heat is generated than a 980nm laser at the same driving current due to lower wall-plug efficiency. Figure 10 shows the calculated heat generation of the 1530nm laser assemblies as a function of CW current. The microchannel liquid cooled package generates about 33W waste heat at the driving current of 24A and the CT mount assembly generates about 14.2W heat at 14A. The maximum heat flux at the die bonding interface (0.2cm by 0.06 cm) is about 2750 W/cm^2 and 1180W/cm^2, respectively, for the microchannel liquid cooled and conduction cooled CT mount packages. This requires efficient and high capacity cooling.

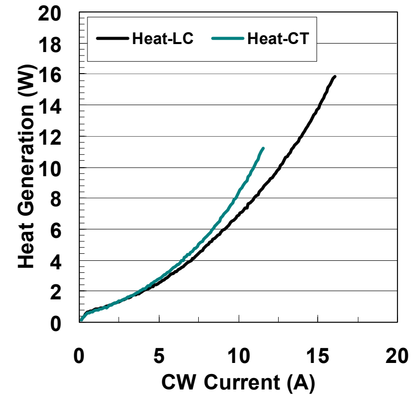

Figure 9. Calculated heat generation of the 980nm laser assemblies as a function of CW current.

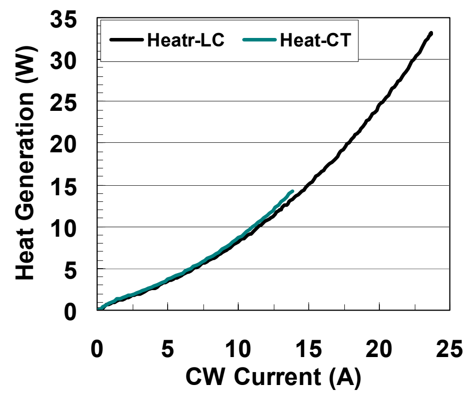

Figure 10. Calculated heat generation of the 1530nm laser assemblies as a function of CW current.

The thermal resistance of the semiconductor laser assemblies can be measured by different methods [1]. In this study, the thermal resistance of the 980nm broad area laser packages was measured using the wavelength method. Figure 11 shows the thermal resistance of microchannel liquid cooled and conduction cooled CT mount packages. The error bars are the standard deviation from three samples. For comparison, we also made p-up bonded CT mount assemblies. The thermal resistance is 2.8K/W, 4.6K/W and 7.8K/W, respectively, for microchannel liquid cooled assembly, conduction cooled CT mount and p-up bonded conduction cooled CT mount package. Clearly the microchannel liquid cooled package has the lower thermal resistance than CT mount assembly due to the more efficient cooling and low thermal resistance contribution from the heatsink. P-up bonding added additional thermal resistance as a result of the contribution from the semiconductor substrate which is 150µm thick.

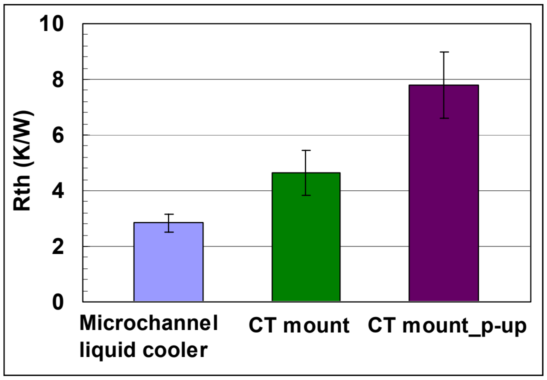

Figure 11. Comparison of the thermal resistance of different package configurations.

Far Fields

The beam quality of high power broad lasers is of great importance for small spot size and efficient coupling. Also beam shape could cause facet damage and reliability concerns. The far fields of the 980nm and 1530nm broad area lasers have been investigated under CW and pulsed current conditions.

Figure 12 shows the typical far field patterns of a microchannel liquid cooled 980nm laser package under CW operation from 1A to 12A and Figure 13 is the typical far field patterns of a 980nm laser package under pulsed current condition of pulse width of 1μs and frequency of 2 kHz from 1A to 20A. We can see that under CW operation, the fast axis (vertical) far field pattern is single mode and the slow axis (horizontal) far field pattern is multimode. The vertical far field patters of CW and pulse operation are similar, while the horizontal far field patterns of CW and pulse operation is very different. The CW horizontal far field patterns have a lot of spikes, but the pulse ones are fairly uniform. It is believed that the elevated junction temperature due to heat generation in the laser greatly enhance the lateral index confinement which leads to existence of many multimodes in the lateral direction. The overlap of these modes creates a non-uniform light pattern at the output facet which could cause facet damage if a high amount of light is concentrated on a small spot in the facet. The full width half maximum (FWHM) divergence of the far fields can be calculated from Gaussian fitting of the far field patterns. The curve fitting of the vertical far field patterns were pretty good, but it was not as good for horizontal far field pattern (especially under CW operation) since the horizontal far field pattern is multimode and is not completely Gaussian shape. However, it does give us a good indication of the divergence angle change with driving current and comparison of different packages. Our results showed that the fast axis divergence angle is very close for both CW and pulsed operation and it remains fairly constant over the operation current range. The fast axis FWHM divergence angle of our 980nm broad area lasers is about 20 degrees. Figure 14 summarizes the typical horizontal far field FWHM divergence angle as a function of driving current of different package configurations and measurement conditions. As can be seen from horizontal far field patterns in Figure 12 (b) and Figure 13 (b) as well as FWHM divergence angle as a function of driving current in Figure 14, the slow axis divergence angle increases significantly with the increasing driving current. For all the packages and both CW and pulsed current conditions, the divergence increases fast initially with increasing current (below 2A) and the increase rate slows down at higher driving currents. Initially the horizontal divergence increase rate is similar for all package configurations under both CW and pulse operation. However, it is very dependent on package configuration under CW operation at high driving currents. The higher the thermal resistance of the package, the faster the horizontal divergence increase with driving current. Under pulsed operation, the horizontal divergence is independent of package configuration and it is normally lower than that under CW operation at the same driving current within calculation error. Because the microchannel liquid cooled package has very low thermal resistance and efficient cooling, the horizontal divergence is fairly close to that of pulsed current operation until up to 7A. The results indicate that it is important to reduce the junction temperature (reduce thermal resistance and/or heat generation) in order to control the horizontal divergence increase.

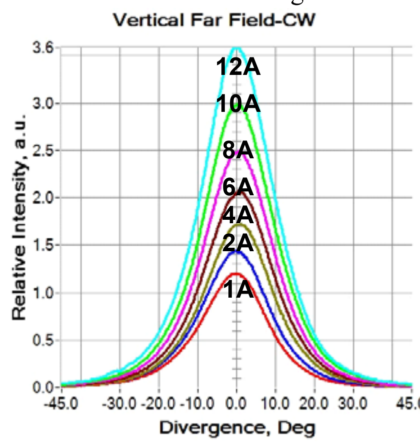

(a)

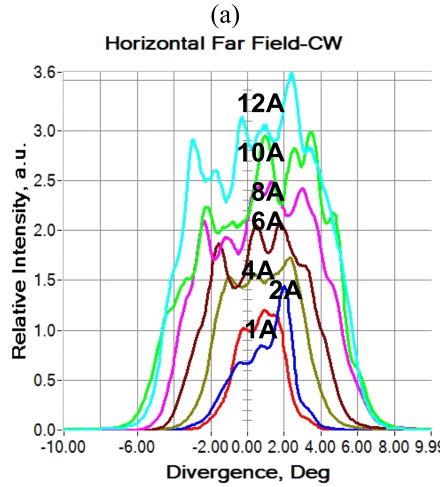

(b)

Figure 12. Typical far field patterns of a microchannel liquid cooled 980nm laser package measured under CW condition; (a) vertical and (b) horizontal.

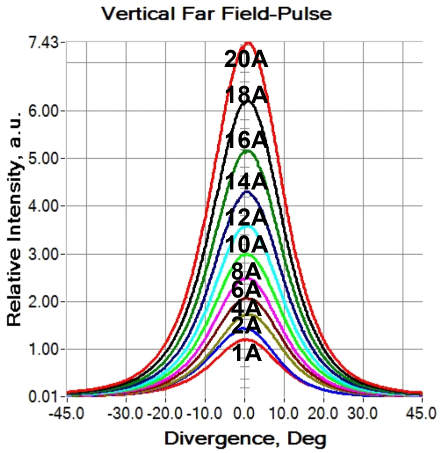

(a)

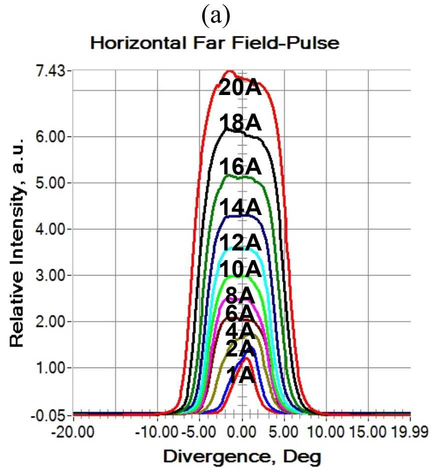

(b)

Figure 13. Typical far field patterns of a 980nm laser package measured under pulsed current condition (pulse width=1µs, frequency=2 kHz); (a) vertical and (b) horizontal.

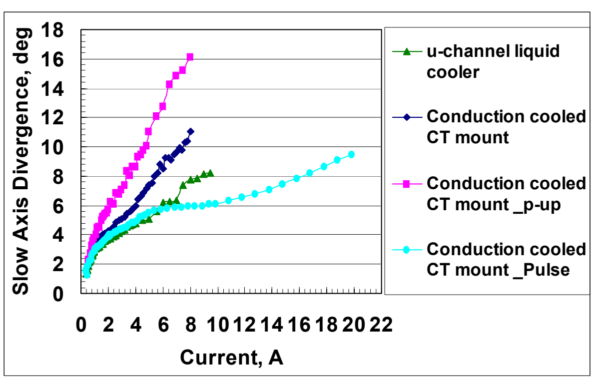

Figure 14. Comparison of the horizontal far field FWHM divergence angle as a function of driving current of different package configurations and measurement conditions.

Similar far field study also was done on 1530nm broad area lasers. The far fields were characterized up to 14A under CW operation and up to 36A under pulsed current condition on CT mount packages. Figure 15 summaries the far field divergence change versus driving current. The results showed that the fast axis divergence of 1530nm lasers barely changes with current and it is normally between 20 and 22 degrees. Again the slow axis divergence increases significantly with the increasing current. Different pulse widths have different slow axis divergence dependence on the current. Obviously the slow axis divergence is related to junction temperature (the amount of heat generated).

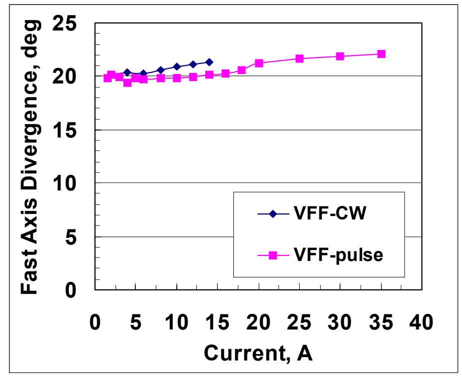

(a)

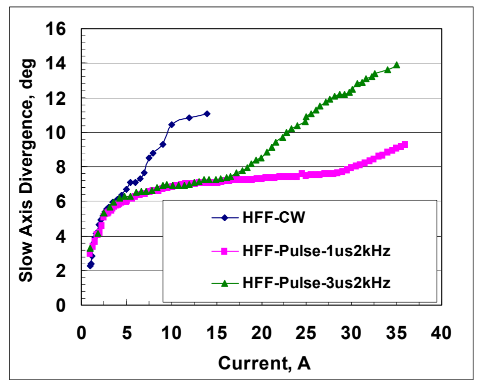

(b)

Figure 15. FWHM divergence versus driving current of a 1530nm CT mount package (a) vertical far field; (b) horizontal far field under CW and pulse (different pulse width) conditions.

Reliability

The reliability of 980nm broad area lasers on conduction cooled CT-mount assembly was evaluated. Indium and AuSn are the solders most commonly used in broad area laser die attachment. Each solder has its advantage and disadvantages. In our study, both solders were used for die bonding and were evaluated. Two lifetime test conditions were used which are 6A and 35 °C, and 7A and 40 °C. At 6A and 35 °C, the average initial optical power of the devices is about 5.3W and it is about 6.2W at 7A and 40C. Figure 16 shows the relative optical power vs. aging time of the CT mount laser assemblies bonded with indium and AuSn solders under both aging conditions. For the 6A and 35 °C test condition, total 10 devices were evaluated. Six of them were indium bonded and the other four were AuSn bonded. For the second condition, eight devices of each solder were tested. From Figure 16 we can see that the indium bonded lasers have much shorter lifetime than AuSn bonded laser under both test conditions. All of the six indium bonded devices failed before 500 hours and all four AuSn bonded ones survived 2300 hours under 6A and 35 °C. Similarly, all the eight indium bonded laser failed before 300 hours under the higher stress condition of 7A and 40 °C, while the AuSn bonded devices have not failed up to 1500 hours. Observation from optical microscope and scanning acoustic microscope (SAM) imaging during the lifetime test, as well as scanning electron microscope (SEM) and energy dispersive x-ray (EDX) analysis of the failed samples showed that severe indium solder electromigration occurred and escalated during lifetime testing for the indium bonded lasers, while AuSn solder did not have detectable electromigration during the lifetime testing time of this study. Figure 17 shows some example images of indium bonded laser CT mount during lifetime test and Scanning Acoustic Microscope (SAM) image after 370 hours of aging. From these images, we can see that the indium electromigration was clearly observed. A pile of indium gradually gathered and then grew at the front side of the CT mount right below the chip during lifetime test. SAM imaging after 370 hours lifetime testing showed that voids have been formed in the indium solder layer, especially at the front of the chip. It is concluded that indium solder is not suitable for very high power laser applications due to electromigration at high current densities and high temperatures and AuSn solder should be used to achieve high reliability for high power laser products.

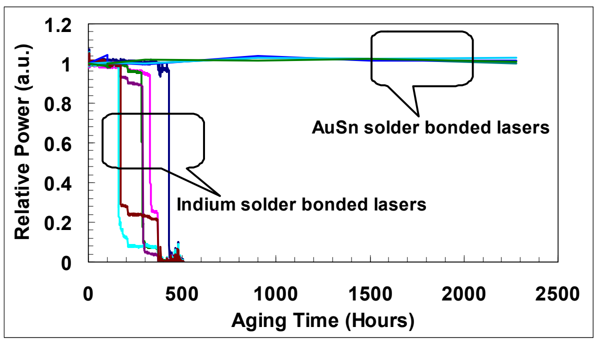

(a)

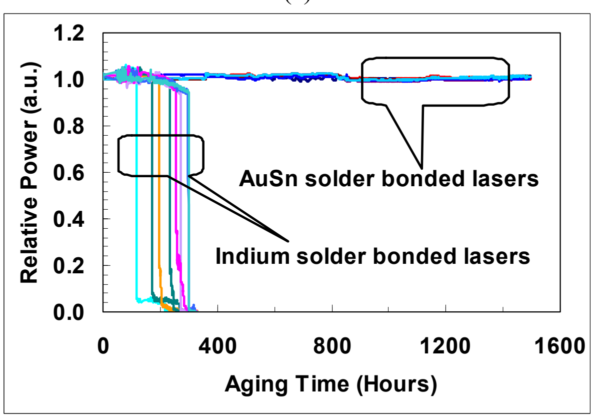

(b)

Figure 16. Relative optical power vs. aging time of the CT mount laser assemblies bonded with indium and AuSn solders under the aging conditions of (a) 6A and 35°C and (b) 7A and 40°C.

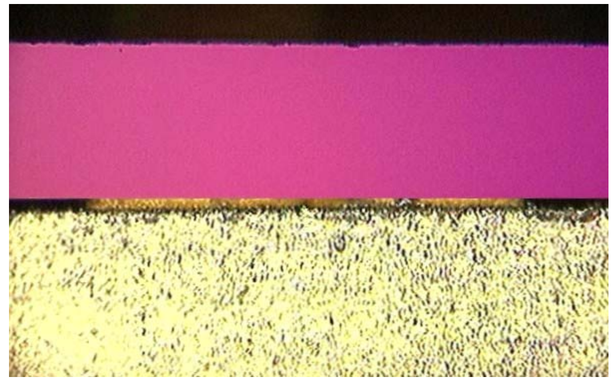

After 50 hours

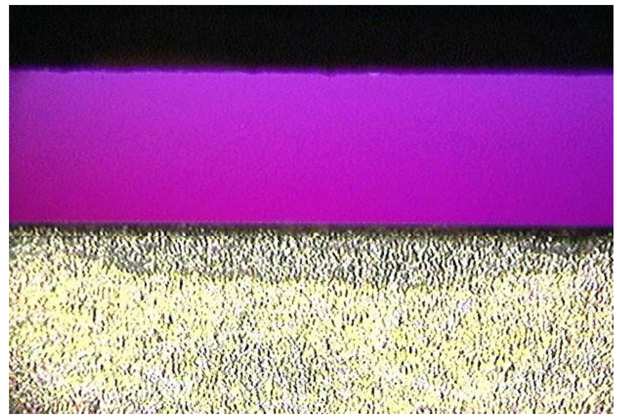

After 290 hours

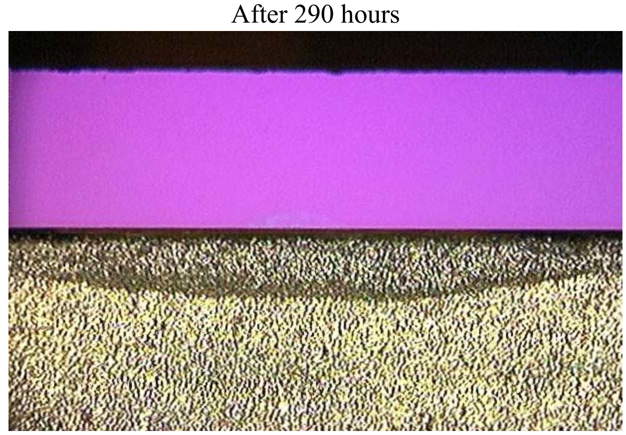

After 370 hours

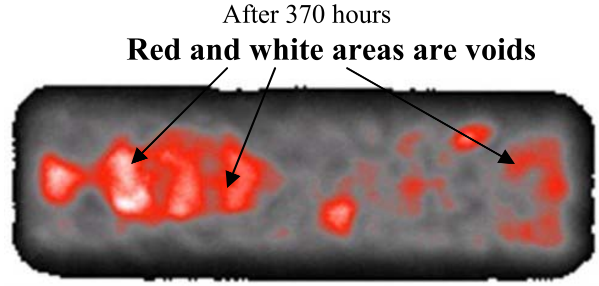

Scanning Acoustic Microscope (SAM) image

Figure 17. Images of indium bonded laser CT mount during lifetime test and Scanning Acoustic Microscope (SAM) image after 370 hours of aging.

Summary and Conclusions

An optical power >7.5W was obtained for the first time from a 1530nm broad area laser with 120 μm stripe width and >15W optical power was achieved from a 980nm broad area laser with the same stripe width, both in microchannel liquid cooled assemblies. For conduction cooled CT-mount packages, >4.5W and >10W were achieved for 1530nm and 980nm lasers, respectively. Furthermore, a high power of 6.5W out of fiber was demonstrated from a pigtailed, fully packaged butterfly-type module without TEC (Thermoelectric cooler). The far fields of the 980nm and 1530nm broad area laser packages have been studied under CW and pulsed current conditions. It was concluded that the junction temperature has a pronounced effect on the beam divergence and far field distribution. The measurement results showed that excellent thermal management through package structure design as well as quality die attachment is the key in not only improving output power, but also significantly improving beam quality for better fiber coupling efficiency and reliability. The reliability evaluation of indium and AuSn solder bonded CT mount assemblies showed that the die attach solder can significant impact the reliability of high power broad area lasers and it was concluded that indium solder is not suitable for high power laser applications due to electromigration at high current densities and high temperatures and that AuSn solder should be used to achieve high reliability for high power laser products.

[1] Xingsheng Liu, Martin Hai Hu, Hong Ky Nguyen, Catherine G. Caneau, Michael H. Rasmussen, Ronald W. Davis, and Chung-En Zah, "Comparison between Epi-Down and Epi-Up Bonded High Power Single-Mode 980 nm Semiconductor Lasers," IEEE Transactions on Advanced Packaging, Vol. 27, No. 4, pp. 640-646, 2004

[2] M. H. Hu, X.S. Liu, and C.E Zah, "Transient and Static Thermal Behavior of High Power Single-Mode Semiconductor Lasers," Proceedings of SPIE, Vol. 4905, pp. 32-36, Shanghai, China, 2002 (Invited paper).

[3] Olivier J. F. Martin, Gian-Luca Bona, and Peter Wolf, "Thermal Behavior of Visible AlGaInP-GaInP Ridge Laser Diodes," IEEE Journal of Quantum Electronics, Vol. 28, No. 11, pp. 2582 –2588, 1992.

[4] Xingsheng Liu, Kechang Song, Ronald W. Davis, Lawrence C. Hughes, Martin H. Hu and Chung-En Zah, "A Metallization Scheme for Junction-Down Bonding of High Power Semiconductor Lasers," to appear in IEEE Transactions on Advanced Packaging.

[5] K. Mizuishi, "Some aspects of bonding-solder deterioration observed in long-lived semiconductor-lasers - solder migration and whisker growth," Journal of Applied Physics, 55 (2): 289-295 1984.

[6] C. C. Lee, C. Y. Wang, and G. S. Matijasevic, "A new bonding technology using gold and tin multilayer composite structures," IEEE Transactions on Components, Hybrids, and Manufacturing Technology, Vol. 14, pp. 407-412, 1991.

[7] C. E. Zah, R. Bhat, C. Caneau, M. Hu, X. Liu, H. K. Nguyen, K. Song, Y. Li and N. Visovsky, "High power 980-nm pump lasers," Technical Report of IEICE, Vol. 103, No. 525, pp21-24, December, 2003.

[8] G.M. Smith, G. Yang, M.K. Davis, S.D. Solimine, R. Bhat, W. Liu, D.A.S. Loeber, F. Yang, A. Kussmaul, M.H. Hu, X.S. Liu, and C.E. Zah, "Design, Performance, And Reliability of 980 nm Pump Lasers," Proceedings of the 16th Annual Meeting of the IEEE Lasers & Electro-Optics Society, Vol. 1, pp. 417-418, Oct. 27-28, 2003, Tucson, AZ.